Highly Sensitive and Transparent Surface Enhanced Raman Scattering Substrates Made by Active Coldly Condensed Ag Nanorod Arrays

ARTICLE *in* THE JOURNAL OF PHYSICAL CHEMISTRY C · SEPTEMBER 2012

Impact Factor: 4.77 · DOI: 10.1021/jp305061s

6 AUTHORS, INCLUDING:

Jitendra P Singh
Indian Institute of Technology Delhi
81 PUBLICATIONS **889** CITATIONS
SEE PROFILE

Ralph Tripp
University of Georgia
211 PUBLICATIONS **10,556** CITATIONS
SEE PROFILE

W. M. Dennis
University of Georgia
87 PUBLICATIONS **998** CITATIONS
SEE PROFILE

THE JOURNAL OF PHYSICAL CHEMISTRY C

Article

pubs.acs.org/JPCC

Highly Sensitive and Transparent Surface Enhanced Raman Scattering Substrates Made by Active Coldly Condensed Ag Nanorod Arrays

J. P. Singh,[†,‡,*] Thomas E. Lanier,[§] Hao Zhu,[§] William M. Dennis,[§] Ralph A. Tripp,[†] and Yiping Zhao[§]

[†]Department of Infectious Diseases, Nanoscale Science and Engineering Center, University of Georgia, Athens, Georgia 30602, United States

[‡]Physics Department, Indian Institute of Technology Delhi, Hauz Khas, New Delhi 110016, India

[§]Department of Physics and Astronomy, Nanoscale Science and Engineering Center, University of Georgia, Athens, Georgia 30602, United States

Supporting Information

ABSTRACT: We report a simple and robust method to fabricate highly sensitive and transparent silver nanorod (AgNR) array substrates for surface enhanced Raman scattering (SERS) using low temperature oblique angle deposition technique. These highly sensitive AgNR SERS substrates consist of tilted AgNRs deposited on glass slides at a substrate temperature T = 140 K. The results show that the substrate temperature plays a crucial role in determining both the morphology and the length of AgNRs. The SERS enhancement activity of these substrates was determined using *trans*-1,2-bis(4-pyridyl) ethylene as a Raman probe molecule. The highest SERS response was obtained from 1 μm long AgNRs fabricated at T = 140 K. Such a deposition reduces the deposition time to 1/4 when compared to similar length AgNRs deposited at room temperature. The effect of the manifestly different surface morphology of low temperature deposited AgNRs on the SERS enhancement is demonstrated by finite-difference time-domain calculations of local field enhancements. The AgNRs arrays grown at 140 K exhibit uniform SERS response and good optical transmission and are cost-effective, which makes this fabrication method a practical choice as a next generation alternative for SERS substrate fabrication.

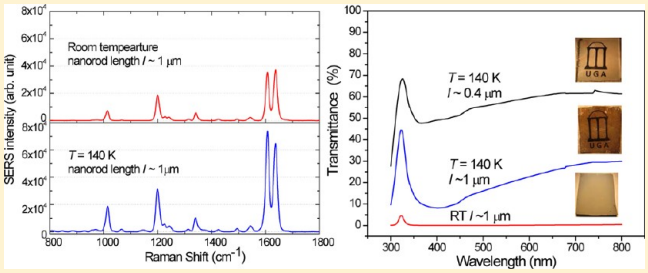

1. INTRODUCTION

Surface enhanced Raman scattering (SERS) is an optical spectroscopic technique in which the excitation of the localized surface plasmon resonance of a nanostructured surface could greatly enhance the local electric fields and amplify the Raman scattering cross-section of molecules attached to those noble metal (such as gold and silver) nanostructures.[1−3] SERS offers an enormous enhancement (>10^6 times) over the traditional Raman signal intensity, a feature that has made this technique an ultrasensitive label free analytical tool to identify very low analyte concentrations of chemicals and biological molecules, even at the single molecule level.[4−7] One of the most important issues concerning the practical application of SERS is to develop a simple and economical batch process to fabricate uniform, reproducible, and highly sensitive SERS substrates. It is important to control all of the factors influencing SERS response in order to maximize signal strength and ensure reproducibility. These factors include the material deposited on the substrate surface; the size, shape, length, and spacing of the deposited nanomaterial; and the corresponding microenvironment. Substantial literature exists in the area of fabrication of SERS substrates,[8−28] but only a few methods are available to develop a uniform, reproducible, robust, stable, and cost-effective SERS substrate. Most of these fabrication methods focus on achieving large enhancement factors but fail to perform in a reproducible manner, which is needed for practical SERS sensors. We have recently shown that oblique angle vapor deposition (OAD) can be used to prepare aligned silver nanorod (AgNR) arrays with a large SERS enhancement factor (>10^8).[29−34] OAD is based on a conventional physical vapor deposition principle and can be used to fabricate aligned and tilted AgNR arrays on large substrate areas. This method involves positioning the substrate at a specific angle such that the vapor flux from the source is incident on the substrate at an oblique angle (>75°). This process produces a geometric shadowing effect that results in the preferential growth of nanorods on the substrate toward the direction of the deposition. The OAD technique offers an easy, straightforward, and inexpensive method for the fabrication of AgNR arrays for high sensitivity SERS applications. SERS substrates produced by OAD have the added advantages of uniformity and reproducibility. We have previously reported less than 12%

Received: May 24, 2012
Revised: August 8, 2012
Published: September 4, 2012

   dx.doi.org/10.1021/jp305061s | J. Phys. Chem. C 2012, 116, 20550−20557

variability for point-to-point intrasubstrate assessment, 6−13% for the intersubstrate assessment from a single fabrication batch, and less than 15% for interbatch variability.[32,34]

Most SERS substrates fabrication processes, including OAD, produce SERS substrates, which are opaque to the visible light. In some specific applications, such as with biological substances, opaqueness of the SERS substrate impedes the visualization of the microscopic details of the biological substances. The optical inspection of biological samples in general is performed by phase contrast microscopy, which is usually performed in a transmission mode where the phase variation is conserved; by contrast the phase variation could be easily disrupted by nonuniform surface reflection in a reflected optical microscope. Therefore, a transparent SERS substrate is required for simultaneous optical examination of specific biological samples and their SERS characterization. Recently, Wang et al.[35] have reported the fabrication of transparent Ag nanoparticle based SERS substrates by oxidizing alumina template by ion-drift processing method. Their transparent SERS substrates suffer from comparatively lower sensitivity, in addition multistep processes involved.

The SERS enhancement factor of AgNR structures is known to be dependent on the morphology of the nanostructures.[34] Recently, Khare et al.[36] have studied the effect of elevated substrate temperature on the morphology and crystallinity of AgNR structures grown by glancing angle deposition. Their results show that at higher substrate temperatures (~623 K), the crystallinity of AgNRs improves but the morphology also changes significantly. In contrast, the surface morphologies of films grown at low substrate temperatures where equilibration is limited have revealed some surprising features. For example, the growth of silver films shows a dependence of surface roughness on the deposition temperature over a range from 55 to 300 K.[37] There have been studies in the past examining SERS measurements on cold-deposited Ag films by Otto and co-workers[38−41] as well as by other researchers.[42−45] However, in a recent study by Albano et al.,[45] the authors systematically analyzed SERS activity of Ag films deposited at substrates temperatures ranging from 58 to 330 K. These cold-deposited Ag films were observed to be highly porous, and studies showed that the pores within the film functioned as the active sites for SERS enhancement.

In this study, we report the fabrication of aligned AgNR array SERS substrates deposited by low temperature oblique angle deposition (LTOAD). These low temperature (LT) SERS substrates exhibit better SERS enhancement with good optical transmission compared to the standard room temperature (RT) deposited AgNR SERS substrates. LT and RT deposited AgNR SERS substrates are compared in terms of spatially averaged local electric field enhancements calculated by the finite-difference time-domain (FDTD) method. Surprisingly, we observed that the AgNR grows much faster at LT (140 K) deposition compared to RT deposition, a feature which results in about 4-fold reduction in the net deposition time of AgNR arrays SERS substrates. These findings show a significant advancement for SERS substrate fabrication and provide a path forward for lowering costs and reducing the amount of silver required to achieve robust and sensitive AgNR SERS substrates.

2. EXPERIMENTAL SECTION

The SERS-active AgNR arrays were fabricated by OAD technique using a custom-designed electron beam evaporation (E-beam) system. Prior to deposition, the glass slides were cleaned using hot piranha solution (80% sulfuric acid, 20% hydrogen peroxide) and then rinsed in deionized water. The substrates were dried with a stream of nitrogen gas before loading into the E-beam evaporation chamber. The source material for evaporation was Ti pellets (Kurt J. Lesker, Clariton, PA, 99.995%) and Ag pellets (Kurt J. Lesker, Clariton, PA, 99.999%). A special copper block sample holder was designed for LTOAD. The copper block sample holder was cooled using a close-cycle liquid nitrogen (LN_2) pumping system attached to the sample holder via two stainless steel bellows connected to a 2.75″ CF tubular feed in the OAD chamber. A K-type thermocouple was directly mounted on the copper sample holder block for in situ temperature measurements. The 1 × 1 cm^2 glass substrates were mounted onto the copper block sample holder using double-sided conducting copper tape. During fabrication, the film thickness was monitored by a quartz crystal microbalance (QCM) positioned at normal incidence to the vapor source direction, and all of the QCM readings and thickness were measured at room temperature. The deposition pressure was ~5× 10^{-7} Torr. Base layers of 20 nm titanium and 200 nm silver films were first evaporated onto these glass substrates at a normal angle to the substrate surface at a rate of 0.2 and 0.3 nm/s, respectively. The substrates were then rotated to 86° with respect to the vapor incident direction and AgNRs were grown at this oblique angle by depositing a desired thickness of silver (as reported by the QCM) with a deposition rate of 0.3 nm/s. During OAD the substrate temperature T was kept constant at 140 K.

The morphology of AgNR films was studied by scanning electron microscopy (SEM). The transmittance spectra of the as-deposited substrates were measured by a Jasco 570 UV−vis spectrometer system in a wavelength range between 300 and 800 nm. A cleaned glass substrate was used as reference in transmittance measurements. For transmission measurements, AgNRs were directly deposited on glass at 140 K without Ti and Ag base layers. The Ag base layer is only 200 nm thick, so we expect a negligible temperature difference on the glass substrate with and without the 200 nm thick Ag base layer. The SERS activity of the coldly condensed AgNR arrays substrates was probed using *trans*-1,2-bis(4-pyridyl) ethylene (BPE, 99.9+ %, Sigma) molecules. BPE solutions were prepared by sequential dilution in ACS grade methanol (Fisher Scientific). A 2 μL droplet of 10^{-5} M BPE solution was applied onto each AgNR substrate, which spread and covered the entire substrate uniformly, and allowed to dry before the acquisition of spectral data. The SERS spectra were acquired using a confocal Raman microscope system (Senterra, Bruker) interfaced to a thermo-electrically cooled CCD-equipped spectrograph. A near-infrared laser at a wavelength of 785 nm was used as the excitation source, and spectra were collected using 48 mW laser power and a 10× objective. The integration time was 10 s. The SERS spectra were collected from multiple points across the BPE-treated portion of the AgNR film.

3. RESULTS AND DISCUSSION

3.1. Morphology Characterization of RT and LT Deposited AgNR Arrays. Figure 1 shows the top view SEM images of Ag nanostructured films grown at RT (Figure 1a) and at T = 140 K (Figure 1b) for the same QCM thickness reading of 2 μm. The surface morphology changes drastically for the LT deposited Ag nanostructured film (Figure 1b). An important difference detectable among the substrates morphology is the presence of nanosize holes in the LT deposited Ag

dx.doi.org/10.1021/jp305061s | J. Phys. Chem. C 2012, 116, 20550−20557

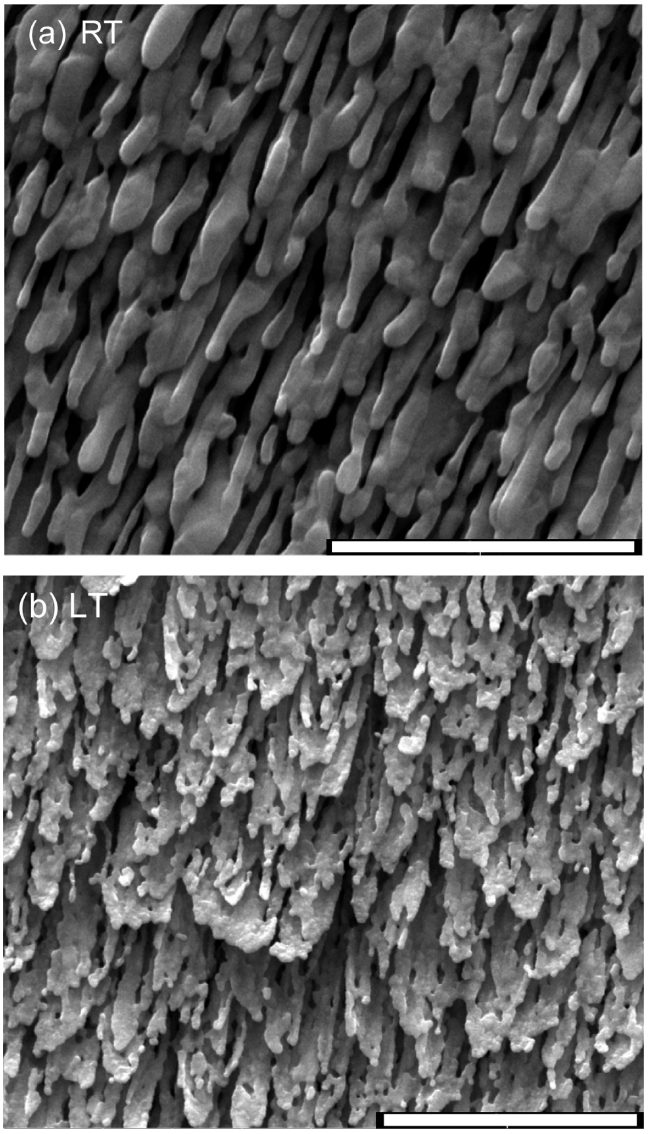

Figure 1. SEM top-view images of AgNR-SERS substrates grown at (a) room temperature and (b) 140 K substrate temperature. The scale bars are of 2 μm.

nanostructured film, whereas RT deposited Ag nanostructured films appear to be solid and rod-like. Other noticeable differences are the formation of blade-like structures at the LT deposited Ag nanostructures tips. The LT deposited Ag nanostructured film appears to be more porous than the Ag nanorods deposited at RT. The side-view SEM images of RT and LT deposited Ag columnar films are shown in Figure 2. The AgNRs were observed to be tilted by angle β with respect to the substrate normal. The tilted ($\beta \approx 65° \pm 2$) AgNRs with an irregular geometry were grown at RT deposition; whereas well-defined tilted ($\beta \approx 63° \pm 1$) fibrous AgNR structures were observed at T = 140 K. The diameter of AgNRs were estimated from SEM side-view images (Figure 2) and ranges between 90 and 110 nm and 50 and 75 nm for RT and T = 140 K depositions, respectively, indicating that LT deposited AgNRs are comparatively thinner. Surprisingly, the lengths of the AgNRs grown at T = 140 K were found to be much longer (more than 3 times) when compared to RT deposited AgNRs under the similar deposition conditions. This finding is of importance because the SERS enhancement of OAD grown AgNRs depends on the nanorod length.[32] The difference in the nanorod length (l) between LT deposition and RT deposition led us to investigate the dependence of l on the QCM thickness reading d. The results in Figure 3 show how the QCM reading affects the length of AgNR grown at T = 140 K. The data show that l increases almost linearly with an increase in the film deposition thickness d. For comparison, data points corresponding to a standard RT optimized SERS substrate is also shown in Figure 3. The effect of substrate temperature is clearly evident where the AgNRs becomes longer with l = 3.5 ± 0.2 μm at T = 140 K compared to l = 1.1 ± 0.1 μm at RT for the same QCM reading of 2 μm. Since the deposition conditions

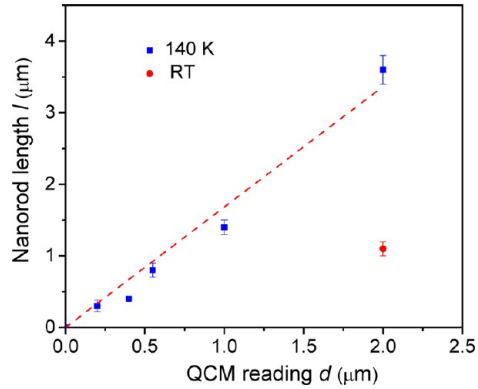

Figure 3. Dependence of AgNR length l measured from SEM micrographs on the deposited film thickness (QCM) for 140 K substrate temperature (solid blue squares) depositions. For comparison, a data point corresponding to standard AgNRs at room temperature (solid red circle) deposition is also shown.

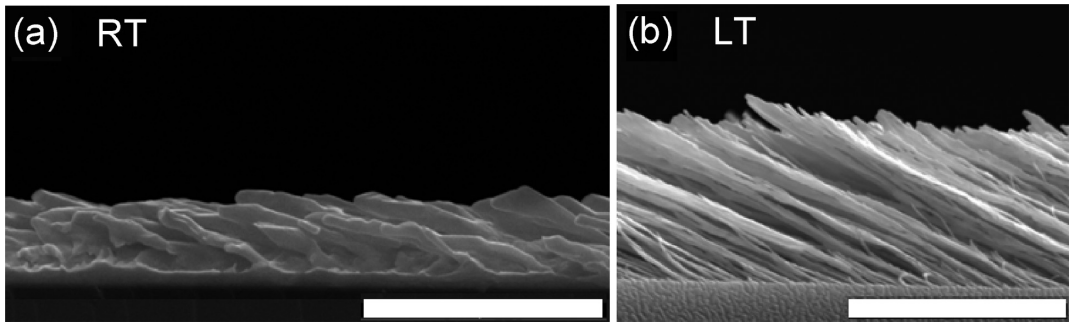

Figure 2. SEM side-view images of AgNR-SERS substrates grown at (a) room temperature and (b) 140 K substrate temperature. The scale bars are of 2 μm.

dx.doi.org/10.1021/jp305061s | J. Phys. Chem. C 2012, 116, 20550−20557

were kept the same for both LT and RT AgNR depositions, the growth rate of nanorod length l was estimated to be 0.50 and 0.16 nm/s, for depositions at T = 140 K and RT, respectively. This clearly shows that at LT the growth rate of nanorod length is about three times larger than similar RT deposition. For low substrate temperatures, the mobility of Ag adatoms on the growing surfaces becomes smaller with a higher sticking coefficient of Ag adatoms at the landing sites.[46] For OAD, the surface diffusion and shadowing are the important physical parameters that control the morphology of the finally grown columnar films. The reduction in the surface diffusion of Ag adatoms at low temperatures results in a comparatively smaller lateral growth of the Ag film and will promote growth of columnar morphology toward the direction of incoming vapor flux. This will cause a net increase in the growth rate of the columnar film and hence, increase in the nanorod length and porosity of LT AgNR film compared to RT deposited AgNR film. Other interesting observations include the formation of blade-like structures at the AgNR tips or apexes (Figure 1b), and the growth of comparatively thinner and well isolated nanorods at lower substrate temperature than deposited at RT. Thus, it appears that LT deposition generates AgNRs composed of large granular structures (Figures 1 and 2). These findings contrast with what is observed during growth at higher substrate temperatures (~600 K) where single crystalline AgNRs were observed.[36] During LTOAD, the incoming Ag adatoms carry momentum and energy which are transferred to the atoms on the depositing surface. The large number of grain boundaries impedes the flow of heat from silver adatoms landing sites to the nanorod bottom by increasing the net thermal resistance path. This results in an increase of the local temperature of the AgNRs tips and enhances the surface diffusion of Ag adatoms on the nanorods apexes at later stages of AgNR growth at T = 140 K. Whereas, RT deposited AgNR substrates are composed of smaller number of grains boundaries that make it easier for the thermal energy to be transported from silver adatoms landing sites to the AgNR bottom and the resulting morphology seem to be more solid rod-like.

3.2. Optical Absorbance/Transmission Measurements. The absorption spectra of AgNR SERS substrates deposited at RT and at T = 140 K are shown in Figure 4. The RT deposited AgNR arrays film shows comparatively narrower surface plasmon (SP) peak at 400 nm than the LT deposited AgNR structures. This may be due to the difference in the average diameter of the RT and LT deposited AgNR structures as discussed above. One of the consequences of the increased porosity in the LT deposited AgNR arrays film to the RT deposited AgNR arrays film is the enhancement in the optical transmission. The transmission spectra and photographs of SERS AgNR substrates deposited at RT and T = 140 K are shown in Figure 5. The transmission peak at 320 nm present in all the transmission spectra is a characteristic peak of bulk silver. Comparing to an opaque AgNRs SERS substrate grown at RT, the AgNRs SERS substrates grown at T = 140 K appear to be brighter and show higher optical transmittance in the spectral range between 300 to 800 nm. For example, similar length ($l \approx 1$ μm) AgNRs deposited at T = 140 K show 28% transmittance at 680 nm, whereas the RT grown AgNRs show almost no transmittance having a value close to zero for all spectral wavelengths examined. Interestingly, the transmittance increases with reduction in the nanorod length, i.e., ~60% transmittance at 680 nm for AgNR length of 400 nm. The increased optical transmittance from the LT AgNR-SERS substrates is due the presence of thinner fibrous AgNRs morphology with an enhanced porosity.

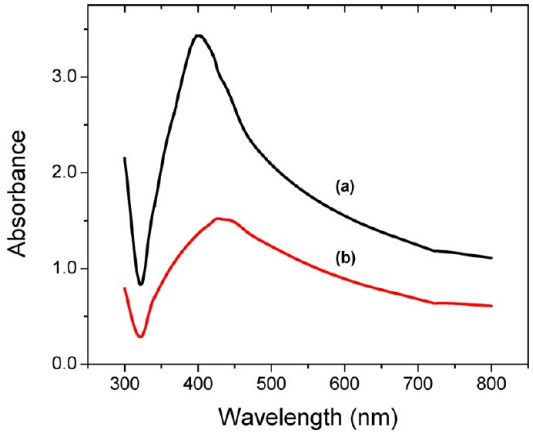

Figure 4. Plots of optical absorbance versus wavelength for AgNR arrays SERS substrates deposited (a) at room temperature and (b) at 140 K substrate temperature with nanorod lengths of $l \approx 1$ μm.

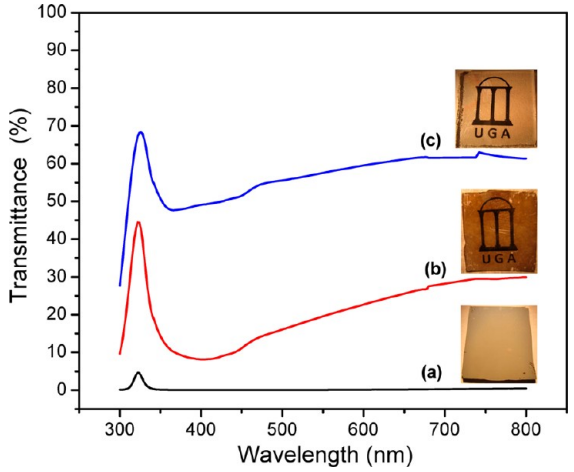

Figure 5. Plots of optical transmittance with wavelength for AgNR arrays SERS substrates deposited (a) at room temperature (nanorod length $l \approx 1$ μm) and 140 K substrate temperature with nanorod lengths of (b) $l \approx 1$ μm and (c) $l \approx 0.4$ μm. The corresponding photographs are also shown.

3.3. SERS Characterizations of RT and LT Deposited AgNR Arrays Substrates. The RT deposited silver nanostructures have been shown to be superior SERS substrates by previous researchers.[12−14,29−32] Thus for a comparison, the SERS response associated with the LTOAD deposited AgNR substrates was determined. The averaged background SERS spectra of bare AgNR arrays deposited at RT and at 140 K substrate temperature are shown in Figure 6a. The averaged SERS spectra of BPE on the AgNR arrays deposited at RT as well as at T = 140 K are shown in Figure 6b. The main bands of BPE at 1015, 1200, 1610, and 1640 cm^{-1} can be assigned to the pyridine ring breathing mode, the ethylenic C═C in-plane ring mode, the aromatic ring stretching mode, and the C═C stretching mode, respectively.[37] The peak around 1350 cm^{-1} can be attributed to amorphous carbon. Vapor deposited silver films and electrochemically reduced silver electrodes have been reported to exhibit backgrounds due to

dx.doi.org/10.1021/jp305061s | J. Phys. Chem. C 2012, 116, 20550−20557

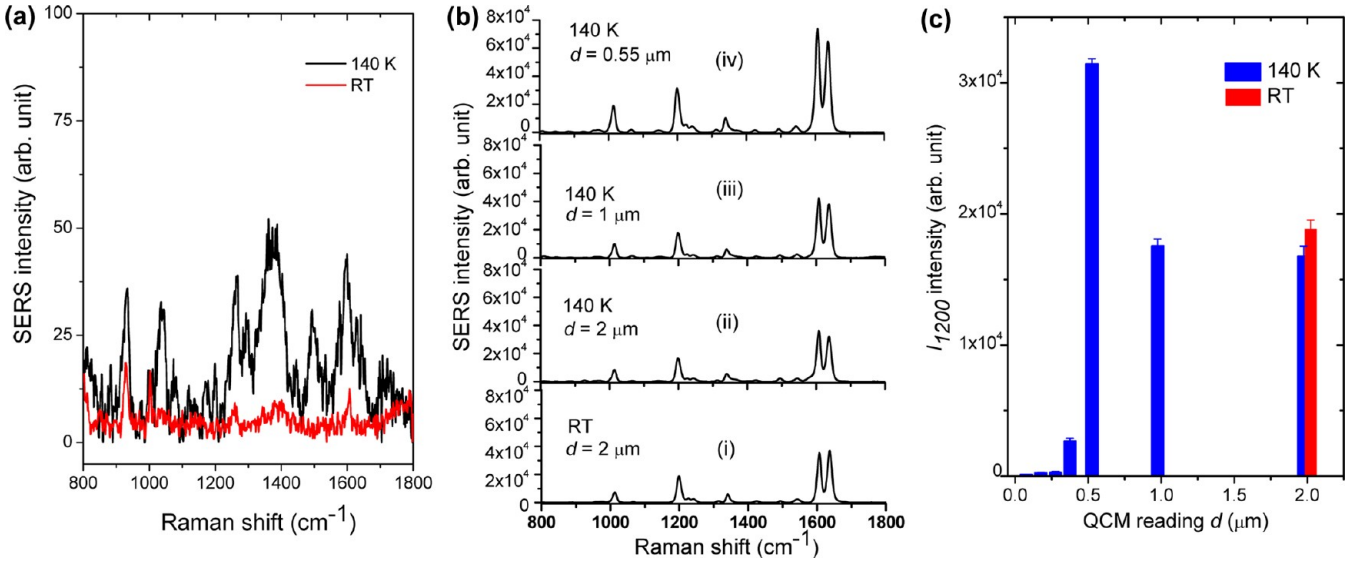

Figure 6. (a) Background SERS spectra of bare AgNR arrays deposited at room temperature and at 140 K substrate temperature for QCM reading d values of 2 and 0.55 μm, respectively. (b) SERS spectra of 10^{-5} M BPE applied to AgNR arrays deposited at (i) room temperature (d = 2 μm) and at 140 K substrate temperature for d values of (ii) 2, (iii) 1, and (iv) 0.55 μm. The spectra are the average of five different positions measured on each of the sample surfaces. (c) Bar graph showing the dependence of I_{1200} on the QCM reading d deposited at 140 K substrate temperature. A I_{1200} intensity bar corresponding to a room temperature deposited AgNRs-SERS substrate for d = 2 μm value is also shown.

graphitic carbonaceous adsorption onto the substrate. The other comparatively smaller bands in the spectra possibly arise from organic impurities from the ambient environment or outgassing from the deposition chamber. All the spectra were baseline corrected using Bruker's 64-point rubber-band algorithm. An overall increase in the intensity of the SERS signal with decrease in the film deposition thickness d-value was observed for the LT deposited AgNR substrates. It is interesting to notice that the relative intensity of BPE peak at 1610 cm^{-1} is higher than that of 1640 cm^{-1} for RT deposited AgNR arrays substrates whereas it inverts for LT deposited AgNR arrays substrates. Recently, Neaton and co-workers[47] have examined binding of BPE molecules to the Au surfaces and studied variations in the experimental data that arise from the differences in how the BPE molecule binds to the substrate using density functional theory (DFT). The researchers proposed that the BPE molecules adsorbed at different binding sites can alter both relative peak heights (1610 and 1640 cm^{-1}) and the overall peak intensity. Depending upon the binding sites the peak intensity ratio can be inverted. The morphology of Ag nanostructures grown at low temperatures (Figure 1b) is very different from the Ag nanostructures deposited on substrates at room temperature. The morphological induced orientation change of BPE molecules on the silver surface may cause difference in the peak intensity of 1610 and 1640 cm^{-1}. SERS can only excite Raman modes with vibrational direction perpendicular to the substrate surface, since the surface E-field is always perpendicular to the substrate surface. Zhuang et al.[48] have calculated different vibrational frequencies of BPE on silver surface using density functional theory. The authors also listed the relative enhancement factor (REF) for different possible SERS modes and have reported a higher REF for SERS peak near 1600 than 1635 cm^{-1} at RT. The baseline-corrected peak height of the BPE peak located at about 1200 cm^{-1} was used to quantify the overall SERS response, and is denoted as I_{1200}. The dependence of film deposition thickness d on SERS peak intensity I_{1200} is illustrated as a bar graph in Figure 6c. The maximum SERS response was obtained for d = 550 nm, whereas SERS response decreases by about 44% and 47% (measured with respect to d = 550 nm value) for d = 1 and 2 μm, respectively. The standard OAD grown RT SERS substrate yields the SERS intensity I_{1200} about 60% of that of the d = 550 nm LT substrate. This is an important finding because the AgNRs SERS substrates grown at T = 140 K not only show the maximum SERS response, but the process also reduces the amount of silver source material required for fabrication providing substantial cost savings. In previous studies, we have extensively studied AgNR parameters such as nanorod length (l), nanorod diameter (D), and deposition angle (θ) on the SERS enhancement factor.[34] It was shown that the maximum SERS intensity was obtained for l = 1 μm long AgNR arrays corresponding to d = 2 μm QCM reading deposited at room temperature.[34] Surprisingly, for AgNR arrays grown at T = 140 K, the maximum SERS intensity I_{1200} (Figure 6c) was also observed for a similar nanorod length of $l \approx 0.9$ μm, but in this case at smaller (about four times less) QCM reading of d = 0.55 μm. The SERS intensity I_{1200} decreases for higher d values that may be attributed to a decrease in the area density of BPE Raman probe molecules with an increase in nanorod length, and hence, surface area of the corresponding nanorod arrays. The SERS measurements were also performed on LTOAD grown AgNR arrays without the silver thin film base layer. An overall decrease of about 15% in the SERS intensity I_{1200} was observed compared to the AgNR array SERS substrates deposited with Ag thin film base layer. For blade-like porous AgNR morphology, an effect induced by low temperature deposition, these AgNRs apexes may introduce extra hot spots for local enhancement of SERS signal intensity. Recently, we have determined the effect of nanorod's geometry such as length, tilt angle, and nanorod diameter on SERS enhancement factor (EF) of AgNR arrays grown at room temperature.[34] The SERS EF shows a strong dependence on the nanorod length and deposition angle. The maximum SERS EF value of 7.2 × 10^8 was observed for the optimum AgNR SERS substrate having a length of about 1 μm. Although, SERS EF was not determined for the LT SERS substrates but it is expected to be

dx.doi.org/10.1021/jp305061s | J. Phys. Chem. C 2012, 116, 20550−20557

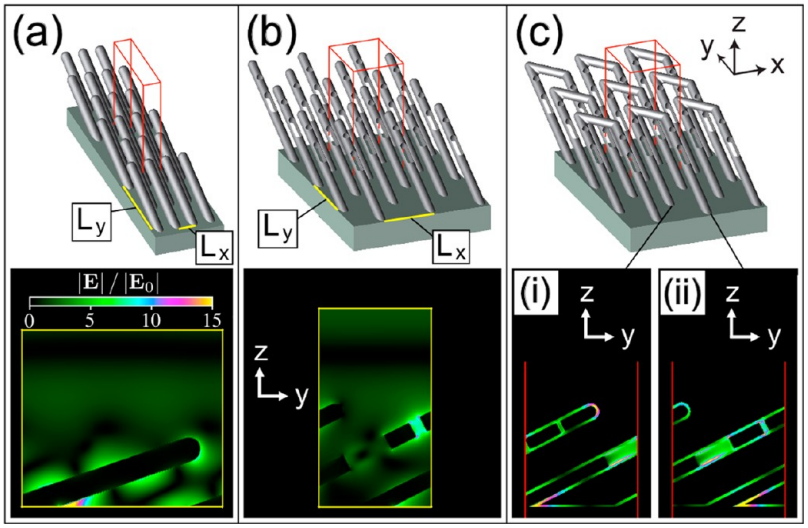

Figure 7. Idealized morphologies used in FDTD simulations and example local field enhancements. The red box indicates the unit cell of each staggered array and defines the computational domain. See text for geometrical parameters. (a) AgNRs deposited by OAD at room temperature. (b) Porous AgNRs deposited by OAD at 140 K substrate temperature. (c) The porous LT morphology with connective rod segments added. Panels (i) and (ii) show slices of the integration volume near the edge of the pores of rods as indicated. Note that the connective segment is not visible in panels (i) and (ii) because the slice does not intersect it in space. The incident wave is *y*-polarized and has amplitude 1.0 (arbitrary units) in all cases. Note that values of the magnitude of the electric field greater than 15 will saturate the color scale, which applies to all plots.

of the similar order. A widely accepted contribution to the measured enhancement of Raman scattering from molecules deposited on metallic nanostructures is the concentration of the electric field in particular localized regions of the surface morphology.[49] These regions are referred to as "hot spots", and their significance is attributed to a scaling of the electromagnetic contribution to the detected Raman-shifted radiation (integrated SERS intensity, I^{SERS}) as the fourth power of the ratio of the local electric field ($\mathbf{E}_{local}(\omega)$) near the metallic surfaces to the incident electric field ($\mathbf{E}_0(\omega)$):[50−52]

$$I^{SERS} \approx \left| \frac{\mathbf{E}_{local}(\omega)}{\mathbf{E}_0(\omega)} \right|^4 \quad (1)$$

The surface morphology of LT deposited AgNRs is characterized by nanosized holes and blade-like structures at the AgNR tips and is different from the conventional AgNR structures grown at room temperature (Figure 1a,b). The SERS signal intensity I_{1200} measured from LT deposited AgNR arrays is larger by a factor of ∼2 relative to AgNR arrays deposited at RT as shown in Figure 6.

3.4. Finite-Difference Time-Domain (FDTD) Modeling. In order to investigate the dependence of the local field enhancement on the observed modifications to the AgNR surface morphology, numerical simulations were carried out using the finite-difference time-domain (FDTD) software package XFdtd (Remcom) (see the Supporting Information S1 for details).[53−55] The RT and LT deposited AgNR substrates were modeled as two-dimensional (2-D) staggered arrays with lattice vectors $L_x\hat{x}$ and $L_y\hat{y}$ to form a 2-D rhombic Bravais lattice. The separations between positions of the AgNRs for the RT case are L_x = 177 nm and L_y = 862 nm, whereas for LT deposited porous AgNRs these parameters take the values L_x = 400 nm and L_y = 500 nm. The effect of increased porosity in LT deposited AgNRs was modeled by inserting 50 nm diameter pores and 50 nm ×200 nm slits into the rods. The AgNRs are positioned on a 200 nm Ag base layer. The laser wavelength of 785 nm was used in the FDTD simulations. Figure 7 shows the idealized morphologies of the tilted AgNRs used in the FDTD simulations and their corresponding local field enhancements ($|\mathbf{E}_{local}/\mathbf{E}_0|$). The 2-D slices in Figure 7 show the electric field magnitude at a point in time which best represents the hot spots in each case. Since the incident electric field has a amplitude 1.0 (arbitrary units), this represents the spatial distribution of the local field enhancement in the slice. A steady-state hot spot is identified near the small-angle point of contact between tilted rods and base layer for the case of a *y*-polarized incident wave (Figure 7(a)). The electric field magnitude reaches a strong maximum (∼60 times the incident amplitude) precisely at the intersection between nanorod and base layer. The field reaches this magnitude only within a very small volume of the idealized surface morphology. For RT AgNRs, our results as depicted in Figure 7a are comparable to the previous numerical investigations of the local field enhancement on similar AgNR structures.[56] The morphology shown in Figure 7b for the LT case exhibits hot spots in and around the pores and slits, with a decreased enhancement at the base owing in part to the smaller tilt angle. Again, maxima (∼20 times the incident amplitude) are found in small volumes located near the sharp material features. It is clear that the magnitude of the electric field has very different and complicated spatial dependence in the two cases. Spatial averaging is therefore necessary to compare in a more meaningful way the electromagnetic contribution to the detected Raman signal computed for the two morphologies.[49,57] The ratio of the averaged Raman scattering enhancement (I^{SERS}_{avg}(LT)/(I^{SERS}_{avg}(RT)) calculated for two different AgNR morphologies provides a quantitative measure of the enhancement of the electromagnetic contribution to the detected Raman signal. It is known that rough and/or porous features on metallic nanostructures lead to enhanced local fields.[58] While the field is enhanced in and around the pores of the structure as shown in Figure 7b, the averaged Raman scattering enhancement (I^{SERS}_{avg}(LT) is not superior to that of (I^{SERS}_{avg}(RT). These results led us to suppose that the blade-type morphology situated predominantly at the rod tips as evident in

dx.doi.org/10.1021/jp305061s | J. Phys. Chem. C 2012, 116, 20550−20557

the SEM image in Figure 1b might play an important role. To test this, the morphology of Figure 7b was simply modified by adding connective rod segments, which lie in a plane normal to the incident propagation vector and connect rods that are staggered with respect to each other. This morphology is shown in Figure 7c. This construction resulted in $I_{avg}^{SERS}(LT)/I_{avg}^{SERS}(RT) \approx 2$. The peak electric field magnitudes in a slice of the integration volume are shown in Figure 7c. It is important to recognize that the contribution to $I_{avg}^{SERS}(LT)$ from the connective rod segments was smaller than the contribution from the other portions of the integration volume. In other words, it is not that the local field is enhanced on the added segment, but rather, that the added segment is, on average, more strongly driven by each orthogonal component of the unpolarized incident field, and provides a conductive pathway between rods which leads to superior local field enhancement near the pores and other sharp features.

SERS enhancement factors depend on all morphological parameters. Performing FDTD calculations using morphologies that precisely replicate the intricate details evident in SEM images would not provide the physical insight into the role of the general features of the morphologies. Although comparison of the results of such an investigation with the experimental results would constitute a test of the validity of eq 1, this was not the purpose of our calculations. The statistically significant plasmonic properties of the nanostructures, spatially averaged over the laser beam spot, were presumed to be identifiable using idealized morphologies with similar attributes, e.g., rod angle, the presence of pores, and connected/nonconnected rod tips. The simulations described in this work focused on the effect of porosity and blade-like connected rod tips by comparing results for idealized morphologies so distinguished. The main findings are that the field enhancement at the pore hot spots is greatly increased by the presence of connected rod tips and that a spatially averaged electromagnetic scattering enhancement superior to that of the RT case requires that the porous rods be interconnected.

4. CONCLUSIONS

The results show that SERS substrates deposited by LTOAD provide an inexpensive way to fabricate highly sensitive and comparatively transparent SERS substrates. The AgNRs grown at $T = 140$ K are longer and more porous than those deposited at RT. We contend that reduction in the adatom mobility along with a higher sticking coefficient of Ag adatoms on the growing surface at low temperature (140 K) results in both an increase in the nanorod length and enhanced porosity. The increase in the optical transmittance of the low temperature deposited AgNRs film is a manifestation of the increase in porosity of the AgNRs film. The pores have been identified as electric field hot spots in our FDTD calculations, which have further demonstrated the significance of the blade-like rod tips to the electromagnetic contribution to SERS enhancement. This study advances SERS substrate fabrication providing a path for producing technologically and functionally superior substrates with the added advantage of cost effectiveness.

■ ASSOCIATED CONTENT

Supporting Information

SERS spectra showing the stability of LT AgNR arrays SERS substrates against storage under ambient conditions and optical micrographs of Vero cells on transparent LT AgNR arrays. SERS substrates and the details of FDTD parameters and the calculation steps used in the determination of Raman scattering enhancements from tilted AgNR structures. This material is available free of charge via the Internet at http://pubs.acs.org.

■ AUTHOR INFORMATION

Corresponding Author

*E-mail: jpsingh@physics.iitd.ac.in.

Notes

The authors declare no competing financial interest.

■ ACKNOWLEDGMENTS

This research work was supported by U.S. Army Research Laboratory under Grant No. W911NF-07-R-0001-04 and National Science Foundation under Contract No. ECCS-1029609.

■ REFERENCES

(1) Stiles, P. L.; Dieringer, J. A.; Shah, N. C.; Van Duyne, R. P. *Annu. Rev. Anal. Chem.* **2008**, *1*, 601.
(2) Tian, Z. Q.; Ren, B.; Wu, D. Y. *J. Phys. Chem. B* **2002**, *106*, 9463.
(3) Campion, A.; Kambhampati, P. *Chem. Soc. Rev.* **1998**, *27*, 241.
(4) Nie, S.; Emory, S. R. *Science* **1997**, *275*, 1102.
(5) Fleischm, M.; Hendra, P. J.; McQuilla, A. *Chem. Phys. Lett.* **1974**, *26*, 163.
(6) Natan, M. J. *Faraday Discuss.* **2006**, *132*, 321.
(7) Hudson, S. D.; Chumanov, G. *Anal. Bioanal. Chem.* **2009**, *394*, 679.
(8) Kahl, M.; Voges, E.; Kostrewa, S.; Viets, C.; Hill, W. *Sens. Actuators B* **1998**, *51*, 285.
(9) Alivarez-Puebla, R.; Liz-Marzan, L. M. *Chem. Soc. Rev.* **2012**, *41*, 43.
(10) Sackmann, M.; Bom, S.; Balster, T.; Materny, A. *J. Raman Spectrosc.* **2007**, *38*, 277.
(11) Billot, L.; de la Chapelle, M. L.; Grimault, A. S.; Vial, A.; Barchiesi, D.; Bijeon, J. L.; Adam, P. M.; Royer, P. *Chem. Phys. Lett.* **2006**, *422*, 303.
(12) Alvarez-Puebla, R.; Cui, B.; Bravo-Vasquez, J. P.; Verse, T.; Fenniri, H. *J. Phys. Chem. C* **2007**, *111*, 6720.
(13) Hulteen, J. C.; Treichel, D. A.; Smith, M. T.; Duval, M. L.; Jensen, T. R.; Van Duyne, R. P. *J. Phys. Chem. B* **1999**, *103*, 3854.
(14) Ormonde, A. D.; Hicks, E. C. M.; Castillo, J.; Van Duyne, R. P. *Langmuir* **2004**, *20*, 6927.
(15) Zhang, X.; Yonzon, C. R.; Young, M. A.; Stuart, D. A.; Van Duyne, R. P. *IEEE Proc. Nanobiotechnol.* **2005**, *152*, 195.
(16) Haynes, C. L.; McFarland, A. D.; Smith, M. T.; Hulteen, J. C.; Van Duyne, R. P. *J. Phys. Chem. B* **2002**, *106*, 1898.
(17) Kartopu, G.; Es-Souni, M.; Sapelkin, A. V.; Dunstan, D. *Phys. Status Solidi A* **2006**, *203*, R82.
(18) Zhang, L. S.; Zhang, P. X.; Fang, Y. *J. Colloid Interface Sci.* **2007**, *311*, 502.
(19) Ruan, C. M.; Eres, G.; Wang, W.; Zhang, Z. Y.; Gu, B. H. *Langmuir* **2007**, *23*, 5757.
(20) Broglin, B. L.; Andreu, A.; Dhussa, N.; Heath, J. A.; Gerst, J.; Dudley, B.; Holland, D.; El-Kouedi, M. *Langmuir* **2007**, *23*, 4563.
(21) Gu, G. H.; Kim, J.; Kim, L.; Suh, J. S. *J. Phys. Chem. C* **2007**, *111*, 7906.
(22) Lombardi, I.; Cavallotti, P. L.; Carraro, C.; Maboudian, R. *Sens. Actuators B* **2007**, *125*, 353.
(23) Jung, D. S.; Lee, Y. M.; Lee, Y.; Kim, N. H.; Kim, K.; Lee, J. K. *J. Mater. Chem.* **2006**, *16*, 3145.
(24) Chan, S.; Kwon, S.; Koo, T. W.; Lee, L. P.; Berlin, A. A. *Adv. Mater.* **2003**, *15*, 1595.
(25) Lin, H. H.; Mock, J.; Smith, D.; Gao, T.; Sailor, M. J. *J. Phys. Chem. B* **2004**, *108*, 11654.
(26) Henley, S. J.; Carey, J. D.; Silva, S. R. P. *Appl. Phys. Lett.* **2006**, *89*, 183120.

(27) Chattopadhyay, S.; Lo, H. C.; Hsu, C. H.; Chen, L. C.; Chen, K. H. *Chem. Mater.* **2005**, *17*, 553.
(28) Suzuki, M.; Maekita, W.; Wada, Y.; Nakajima, K.; Kimura, K.; Fukuoka, T.; Mori, Y. *Appl. Phys. Lett.* **2006**, *88*, 203121.
(29) Fan, J. G.; Zhao, Y. P. *Langmuir* **2008**, *24*, 14172.
(30) Abell, J. L.; Driskell, J. D.; Dluhy, R. A.; Tripp, R. A.; Zhao, Y. P. *Biosens. Bioelectron.* **2009**, *24*, 3663.
(31) Chaney, S. B.; Shanmukh, S.; Dluhy, R. A.; Zhao, Y. P. *Appl. Phys. Lett.* **2005**, *87*, 031908.
(32) Driskell, J. D.; Shanmukh, S.; Liu, Y.; Chaney, S. B.; Tang, X. J.; Zhao, Y. P.; Dluhy, R. A. *J. Phys. Chem. C* **2008**, *112*, 895.
(33) Abell, J. L.; Garren, J. M.; Zhao, Y. P. *Appl. Spectrosc.* **2011**, *65*, 734.
(34) Liu, Y. J.; Chu, H. Y.; Zhao, Y. P. *J. Phys. Chem. C* **2010**, *114*, 8176.
(35) Wang, H. H.; Cheng, T. Y.; Sharma, P.; Chiang, F. Y.; Chiu, S. W. Y.; Wang, J. K.; Wang, Y. L. *Nanotechnology* **2011**, *22*, 385702.
(36) Khare, C.; Patzig, C.; Gerlach, J. W.; Rauschenbach, B.; Fuhrmann, B. *J. Vac. Sci. Technol. A* **2010**, *28*, 1002.
(37) Stoldt, C. R.; Caspersen, K. J.; Bartelt, M. C.; Jenks, C. J.; Evans, J. W.; Thiel, P. A. *Phys. Rev. Lett.* **2000**, *85*, 800.
(38) Otto, A.; Mrozek, I.; Grabhorn, H.; Akemann, W. *J. Phys.: Condens. Matter* **1992**, *4*, 1143.
(39) Eickmans, J.; Otto, A.; Goldmann, A. *Surf. Sci.* **1986**, *171*, 415.
(40) Bornemann, T.; Otto, A.; Frank, K. H.; Reihl, B. *Surf. Sci.* **1988**, *195*, 161.
(41) Holzapfel, C.; Akemann, W.; Schumacher, D.; Otto, A. *Surf. Sci.* **1990**, *227*, 123.
(42) Zhou, Q.; Li, Z.; Yang, Y.; Zhang, Z. *J. Phys. D: Appl. Phys.* **2008**, *41*, 152007.
(43) Douketis, C.; Haslett, T. L.; Wang, Z.; Moskovits, M.; Iaonnotta, S. *Prog. Surf. Sci.* **1995**, *50*, 187.
(44) Semin, D. J.; Rowlen, K. L. *Anal. Chem.* **1994**, *66*, 4324.
(45) Albano, E. V.; Daiser, S.; Ertl, C.; Miranda, R.; Wandelt, K. *Phys. Rev. Lett.* **1983**, *51*, 2314.
(46) Roda, H.; Brune, H.; Bucher, J. P.; Kern, K. *Surf. Sci.* **1993**, *298*, 121.
(47) Zayak, A. T.; Choo, H.; Hu, Y. S.; Gargas, D. J.; Cabrini, S.; Bokor, J.; Schuck, P. J.; Neaton, J. B. *J. Phys. Chem. Lett.* **2012**, *3*, 1357.
(48) Zhuang, Z.; Cheng, J.; Jia, H.; Zeng, J.; Han, X.; Zhao, B.; Zhang, H.; Zhang, G.; Zhao, W. *Vibr. Spectrosc.* **2007**, *43*, 306.
(49) Le Ru, E. C.; Meyer, M.; Blackie, E.; Etchegoin, P. G. *J. Raman Spectrosc.* **2008**, *39*, 1127.
(50) Vo-Dinh, T. *Trends Anal. Chem.* **1998**, *17*, 557.
(51) Novotny, L.; Hecht, B. *Principles of Nano-Optics*; Cambridge University Press: New York, 2006.
(52) Kerker, M.; Wang, D.-S.; Chew, H. *Appl. Opt.* **1980**, *19*, 4159.
(53) Kunz, K. S.; Luebbers, R. J. *The Finite Difference Time Domain Method for Electromagnetics*; CRC Press: Boca Raton, FL, 1993.
(54) Ordal, M. A.; Long, L. L.; Bell, R. J.; Bell, S. E.; Bell, R. R.; Alexander, J. R. W.; Ward, C. A. *Appl. Opt.* **1983**, *22*, 1099.
(55) Valentine, J.; Zhang, S.; Zentgraf, T.; Ulin-Avila, E.; Genov, D. A.; Bartal, G.; Zhang, X. *Nature* **2008**, *455*, 376.
(56) Liu, Y. J.; Zhang, Z. Y.; Zhao, Q.; Dluhy, R. A.; Zhao, Y. P. *J. Phys. Chem. C* **2009**, *113*, 9664.
(57) Liu, Y.-J.; Zhang, Z.-Y.; Zhao, Q.; Zhao, Y.-P. *Appl. Phys. Lett.* **2008**, *93*, 173106.
(58) Moskovits, M. *Rev. Mod. Phys.* **1985**, *57*, 783.